Chinese Chemical Letters 30 (2019) 911–914

Contents lists available at ScienceDirect

Chinese Chemical Letters

journal homepage: www.elsevier.com/locate/cclet

Communication

Transition metal coordinated framework porphyrin for electrocatalytic oxygen reduction

Chang-Xin Zhao[a], Bo-Quan Li[a], Jia-Ning Liu[a], Jia-Qi Huang[b], Qiang Zhang[a,*]

[a] Beijing Key Laboratory of Green Chemical Reaction Engineering and Technology, Department of Chemical Engineering, Tsinghua University, Beijing 100084, China
[b] Advanced Research Institute of Multidisciplinary Science, Beijing Institute of Technology, Beijing 100081, China

ARTICLE INFO

Article history:
Received 7 March 2019
Received in revised form 13 March 2019
Accepted 15 March 2019
Available online 19 March 2019

Keywords:
Electrocatalysis
Oxygen reduction reaction
Transition metal coordination
Framework porphyrin
Fuel cells

ABSTRACT

Oxygen reduction reaction (ORR) constitutes the core process of many clean and sustainable energy systems including fuel cells and metal–air batteries. Developing high-performance and cost-efficiency ORR electrocatalysts is of great significance to the practical applications of the above-mentioned energy storage devices. Transition metal coordinated porphyrin electrocatalysts are highly considered as a promising substitution of noble-metal-based electrocatalyst because of their high ORR reactivity, where the ORR performances of the porphyrin-based electrocatalysts are highly dependent on the transition metal center. Herein a series of framework porphyrin electrocatalysts coordinated with different transition metal centers (M-POF, where M is Mn, Fe, Co, Ni, Cu, or Zn) was designed, synthesized, and evaluated in regards of electrocatalytic ORR performances. Among all, the Co-POF electrocatalyst exhibits the best ORR performances with the highest half-wave potential of 0.81 V *vs.* RHE and the lowest Tafel slope of 53 mV/dec. This contribution affords an optimized high-performance ORR electrocatalyst and provides instructions for further rational design of porphyrin-based ORR electrocatalysts for sustainable energy applications.

The growing global energy consumption and serious environmental pollution starve for abundant sustainable energy systems [1–5]. Fuel cells and metal–air batteries are promising candidates as next-generation energy storage devices [6–9]. These energy systems require electrochemical reduction of oxygen within the cathode side to supply energy [10–12]. However, the sluggish kinetics of the cathode oxygen reduction reaction (ORR) strongly restricts the actual performances of these energy systems, performing inferior energy efficiency and poor cycling stability [10,13–15]. Therefore, high-performance electrocatalysts are highly required to accelerate ORR, reduce the overpotential, and promote the practical performances of related energy storage devices [16–18]. To date, platinum (Pt)-based electrocatalysts, such as Pt/C, have been identified as the most reactive electrocatalysts for ORR [19–21]. Unfortunately, low abundance and high cost of Pt-based electrocatalysts prohibit their practical applications [19,20]. Developing noble-metal-free electrocatalysts with high electrocatalytic performances is of great significances [22–25].

To replace the impractical Pt-based materials, tremendous studies have been made to develop high-performance noble-metal-free ORR electrocatalysts, including transition metal oxides [26,27], hydroxides [28], carbides [29,30], and sulfides [31,32]. Unfortunately, the practical ORR performances remain unsatisfactory. ORR is a typical surface reaction that the reduction of oxygen takes place at the boundary of the electrode and the electrolyte. Therefore, only surface active sites of the electrocatalyst contribute to the overall ORR performances [33,34]. Based on the above considerations, abundant strategies are proposed to minimize the size of the electrocatalyst particles for full exposure of surface active sites [35,36]. For example, Dai and co-workers synthesized graphene based Co_3O_4 nanocrystals (~4–8 nm in size) for efficient ORR [37]. On the other hand, developing hierarchical structures to increase the surface area constitutes another reasonable pathway [38]. Nevertheless, the above mentioned strategies are incapable to further minimize the size of electrocatalyst nanoparticles to a molecular or atomic level for maximum utilization of active sites. If high-reactivity ORR active sites are atomically dispersed on conductive substrates, a maximum ORR performance would therefore be achieved [39].

Recently, transition metal coordinated porphyrin-based electrocatalysts have been proposed for high-performance ORR

* Corresponding author.
E-mail address: zhang-qiang@mails.tsinghua.edu.cn (Q. Zhang).

https://doi.org/10.1016/j.cclet.2019.03.026

electrocatalysis [40]. Typically, the coordinated transition metal ions serve as actual active sites where hydroxyl feedstocks are attracted and electrons are transferred. Consequently, the category and chemical condition of the coordinated transition metal ions play the most important role in determining the performed ORR reactivity [41]. Many pioneer works investigated the ORR performances of transition metal ion coordinated porphyrin electrocatalysts [42]. However, the best selection of the transition metal ion remains controversial. Although theoretical simulation affords iron as the most active transition metal center, experimental verification remains a great challenge [43]. One big issue that retards experimental investigation is that small porphyrin molecules are not stable and tend to aggregate during electrochemical evaluation, which increases difficulty in identifying the active sequence of transition metal ions [44]. If the porphyrin molecules can be constructed into stable frameworks that can be uniformly distributed on the surface of conductive scaffolds, experimental evaluation of the ORR reactivity of different transition metal ions can be conducted for an optimized selection of transition metal coordinated porphyrin-based electrocatalysts, serving as an instruction for further electrocatalyst design and optimization.

Covalently linking of organic molecules into defined frameworks has been realized following the direction of reticular chemistry. The strategy developed by Yaghi and co-workers serves as an effective tool to construct organic frameworks with stable structure and endows capability for material hybridization [45]. For instance, boroxine [45], triazine [46], phthalocyanine [47], adamantane [48], and fullerene [49] have been successfully covalently linked into organic frameworks of COF-1, CTF, Pc-PBBA COF, PCTF, and PAF-60, respectively. According to the strategy, we proposed a framework porphyrin (POF) material that is constructed of covalently linked porphyrin units into two-dimensional framework structure for transition metal coordination and conducive scaffold hybridization. Our previous contributions demonstrate the effectiveness of the POF materials with high performances in various energy-related devices including rechargeable Zn–air batteries [50], lithium–sulfur batteries [51], and lithium metal batteries [52]. By introducing POF as the platform material, the ORR reactivity of various transition metal ions can therefore be experimentally compared by POF coordination. Favored by the unique structure of POF, aggregation of small porphyrin molecules and low electronic conductivity can be avoided to reveal the intrinsic ORR reactivity of transition metal coordinated porphyrin-based electrocatalysts.

In this contribution, a series of transition metal ions was coordinated within analogous POF-based electrocatalysts, which were facilely synthesized, characterized in detail, and evaluated in regards of their ORR performances. Concretely, manganese (Mn), iron (Fe), cobalt (Co), nickel (Ni), copper (Cu), zinc (Zn) are selected as the object transition metal ions. Structural characterization and elemental analysis verify similar morphology and transition metal content of the electrocatalysts. Further electrochemical evaluation demonstrates the Co-POF electrocatalyst with the best ORR performance. The highest half-wave potential of 0.81 V *vs.* the reversible hydrogen electrode (RHE) and the lowest Tafel slope of 53 mV/dec were achieved on the Co-POF electrocatalyst. This contribution not only affords an optimized high-performance ORR electrocatalyst, but also provides instructions for further rational design of porphyrin-based ORR electrocatalyst for sustainable energy applications.

Fig. 1 demonstrates the fabrication procedure of M-POF electrocatalysts. Sufficient electron conductivity and full exposure of active sites are of great significance to satisfied ORR performances, as well as, convincing experimental evaluation of the intrinsic ORR reactivity. Correspondingly, graphene was

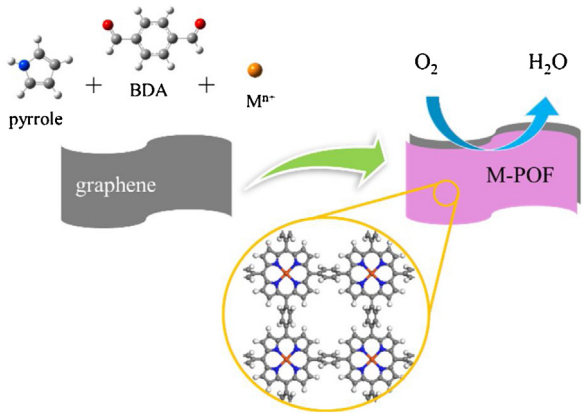

Fig. 1. Schematic illustration of the fabrication procedure of transition metal coordinated framework porphyrin.

introduced as the template to increase the conductivity and regulate the morphology of POF layers from stacking [53]. Following the direct synthesis methodology, M-POF was one-pot synthesized with pyrrole, benzene-1,4-dicarboxaldehyde (BDA), and transition metal salt as substrates. The porphyrin units were constructed by the nucleophilic addition of pyrrole and proton-activated BDA. Corresponding metal ions were simultaneously coordinated within the as-constructed porphyrin units in POF, forming the aimed M-porphyrin active sites for ORR. This synthetic strategy is very easy to follow and serves well to control the morphology of the electrocatalyst and the content of the transition metal ions. The mass ratio of metal coordinated framework porphyrin and graphene was designed to be around 1:3.

Morphology characterization of M-POF was performed using a scanning electron microscope (SEM) and a transmission electron microscope (TEM). All M-POF samples demonstrate similar homogeneous morphology of coated graphene according to SEM images (Fig. 2a and Fig. S1 in Supporting information). On account of the strong intermolecular π–π interactions between graphene and two-dimensional POF sheets, POF is firmly hybridized with graphene with no obvious aggregated or segregated POF. Additionally, TEM images at different magnifications further confirm the uniform hybridization of metal coordinated POF and graphene (Figs. 2b and c, and Fig. S2 in Supporting information). The homogeneous coating of metal coordinated POF on conductive graphene grantees full exposure of active sites toward reactants, which is not only indispensable for excellent ORR performances, but also an essential condition for further electrochemical comparison.

Energy-dispersive X-ray spectrometry (EDS) was carried out for elemental analysis of the M-POF electrocatalysts. All M-POF samples afford similar elemental composition, with reasonable nitrogen contents of between 10 and 20 at% and detectable corresponding transition metal contents (Table 1 and Fig. S3 in Supporting information). For instance, the N and Co content of Co-POF are 15.03 and 0.32 at%, respectively. The element contents are consistent with the molecular design and the material

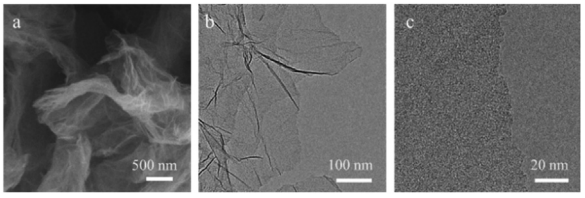

Fig. 2. (a) SEM, (b) TEM, and (c) high-resolution TEM images of Co-POF.

Table 1
Summary of the composition of M-POF electrocatalysts.

Sample	Relative content (at%)			
	Carbon	Nitrogen	Oxygen	Metal
Mn-POF	77.96	21.83	0.00	Mn: 0.21
Fe-POF	89.71	10.85	0.44	Fe: 0.44
Co-POF	84.65	15.03	0.00	Co: 0.32
Ni-POF	83.08	16.51	0.00	Ni: 0.41
Cu-POF	79.74	13.39	5.37	Cu: 1.49
Zn-POF	76.90	21.93	0.00	Zn: 1.17

hybridization of M-POF. Notably, the transition metal elements are ions coordinated within the porphyrin units instead of metal nanoparticles considering the added transition metal salts cannot be reduced to elemental metal in oxidizing and acidic synthetic mediums. The above material characterizations prove the successful fabrication of M-POF electrocatalysts, making ready for the following ORR electrochemical performance evaluation.

Electrochemical measurements were performed using a standard three-electrode system with oxygen-saturated 0.10 mol/L KOH electrolyte at room temperature. The M-POF was individually investigated on a rotating disk electrode (RDE) with a loading of 0.10 mg/cm^2 for the investigation of corresponding ORR electrocatalytic activity. All potentials are calibrated to RHE. 95% *iR*-corrected linear scan voltammogram (LSV) measurements were firstly performed for the investigation of the ORR electrocatalytic activity. As illustrated in Fig. 3a, all M-POF electrocatalysts exhibit similar limiting current density around 4.0 mA/cm^2. Similar limiting current densities suggest mass transportation is similar for all the electrocatalysts, which is attributed to similar morphology. This is important for the comparison of the ORR reactivity of porphyrin coordinated transition metal ions to eliminate the interfere of morphology and mass transportation. Half-wave potential ($E_{1/2}$) is defined as the potential to reach half of the limiting current density, which is considered as the indicator of ORR reactivity [54,55]. As demonstrated, various transition metal ion coordinated M-POF electrocatalysts afford discrepant ORR $E_{1/2}$ (Table 2). Especially, Co-POF exhibits the highest $E_{1/2}$ of 0.81 V *vs.* RHE to render the best ORR reactivity among all the electrocatalysts. In comparison, other M-POF electrocatalysts afford inferior ORR electrocatalytic reactivity. For instance, the $E_{1/2}$ of Mn-POF, Fe-POF, Ni-POF, Cu-POF, and Zn-POF are 0.76, 0.74, 0.69, 0.75, and 0.70 V *vs.* RHE, respectively, 50, 70, 120, 60, and 110 mV lower than the $E_{1/2}$ of the Co-POF electrocatalyst.

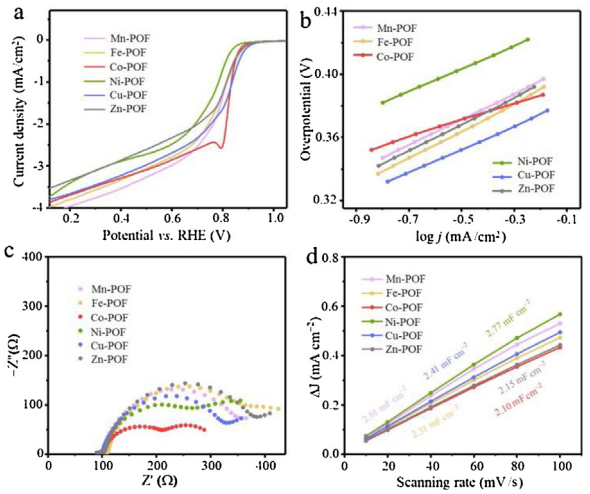

Fig. 3. (a) *iR*-corrected LSV profiles in O_2-saturated 0.10 mol/L KOH (10.0 mV/s), and (b) corresponding Tafel plots, (c) EIS spectrum, and (d) ESCA of M-POF.

Table 2
Summary of ORR performances of M-POF electrocatalysts.

Sample	$E_{1/2}$ (V *vs.* RHE)	Tafel slope (mV/dec)	ESCA (mF/cm^2)
Mn-POF	0.76	81	2.61
Fe-POF	0.74	86	2.31
Co-POF	0.81	53	2.10
Ni-POF	0.69	72	2.77
Cu-POF	0.75	74	2.41
Zn-POF	0.70	85	2.15

Tafel slope is an essential indicator for the measurement of ORR kinetics, which was calculated based on the LSV curves according to the Tafel equation [56]. The Tafel plots in Fig. 3b indicate an identical conclusion as the $E_{1/2}$ indicator suggested that Co-POF possesses the fastest kinetics with the Tafel slope being 53 mV/dec (Table 2). Compared with Co-POF, other M-POF electrocatalysts exhibit inferior ORR kinetics with Tafel slopes of 81, 86, 72, 74, and 85 mV/dec, which are obviously higher than the Tafel slope of Co-POF electrocatalyst. Compared with previously reported noble-metal-free ORR electrocatalysts, the Co-POF electrocatalyst also exhibited advantageous ORR performances with a low overpotential and a small Tafel slope, indicating the Co-POF electrocatalyst among the most kinetically active candidates for the oxygen reduction process (Table S1 in Supporting information).

Additionally, electrochemical impedance spectra (EIS) were performed on the M-POF electrocatalysts. As is distinctly shown in Fig. 3c, Co-POF demonstrates the smallest impedance over other electrocatalysts. The smaller impedance of the Co-POC electrocatalyst suggests the Co-porphyrin structure with better affinity with feedstocks, which further assists rapid charge transfer across the electrocatalyst/electrolyte interface. Considering similar morphology and limiting current density, this may be mainly attributed by the Co-coordination. In addition, M-POF electrocatalysts demonstrate similar electrochemical active surface area (ECSA) at around 2.5 m F/cm^2 (Fig. 3d and Table 2), which excludes ESCA as the reason to the different ORR performances. The evaluation of the ORR electrocatalytic reactivity on different transition metal ion coordinated framework porphyrin electrocatalysts indicates that Co-POF exhibits the best ORR performance. The presented Co-POF electrocatalyst serves well as an excellent ORR electrocatalysts and further implies Co coordination as the favorable selection for porphyrin-based ORR electrocatalysts.

In summary, a series of transition metal coordinated framework porphyrins was prepared and evaluated regarding the ORR electrocatalytic reactivity for an optimized selection of the coordinated transition metal ions. POF was employed as the platform material because of the advantages of its intrinsic two-dimensional structure, well-defined porphyrin units, and strong affinity with conductive graphene templates. Mn, Fe, Co, Ni, Cu, and Zn coordinated POF were molecularly designed, one-pot synthesized, and evaluated in regards of electrocatalytic ORR performances. All M-POF samples exhibit a uniform sheet morphology and expected chemical structure detected by SEM, TEM, and EDS characterization. By evaluating the ORR reactivity of different transition metal ion coordinated POF electrocatalysts, the active sequence was identified from the experimental results. The electrochemical results suggest that Co-POF demonstrates the best ORR electrocatalytic performance with the highest half-wave potential of 0.81 V *vs.* RHE and the lowest Tafel slope of 53 mV/dec. This contribution affords a practical method for the construction of high-performance ORR electrocatalysts, which is expected to be applicable in various energy applications. More importantly, the as-obtained sequence of ORR activity of M-POF electrocatalysts

serves as an instruction towards further rational design of porphyrin-based ORR electrocatalysts.

Acknowledgments

This work was supported by National Key Research and Development Program (Nos. 2016YFA0202500 and 2016YFA0200102), National Natural Science Foundation of China (No. 21825501), and Tsinghua University Initiative Scientific Research Program. We thank Dr. Cheng Tang, Dr. Hao-Fan Wang, and Dr. Bin Wang for helpful discussion.

Appendix A. Supplementary data

Supplementary material related to this article can be found, in the online version, at doi:https://doi.org/10.1016/j.cclet.2019.03.026.

References

[1] X. Ge, A. Sumboja, D. Wuu, et al., ACS Catal. 5 (2015) 4643–4667.
[2] A.A. Gewirth, J.A. Varnell, A.M. DiAscro, Chem. Rev. 118 (2018) 2313–2339.
[3] Y. Guo, P. Yuan, J. Zhang, et al., ACS Nano 12 (2018) 1894–1901.
[4] J. Li, Z. Xi, Y.T. Pan, et al., J. Am. Chem. Soc. 140 (2018) 2926–2932.
[5] H. Yuan, L. Kong, T. Li, Q. Zhang, Chin. Chem. Lett. 28 (2017) 2180–2194.
[6] W.T. Hong, M. Risch, K.A. Stoerzinger, et al., Energy Environ. Sci. 8 (2015) 1404–1427.
[7] Q. Wang, Y. Ji, Y. Lei, et al., ACS Energy Lett. 3 (2018) 1183–1191.
[8] C.Y. Lin, D. Zhang, Z. Zhao, Z. Xia, Adv. Mater. 30 (2018) 1703646.
[9] M. Kiani, J. Zhang, Y. Luo, et al., J. Energy Chem. 27 (2018) 1124–1139.
[10] V.R. Stamenkovic, D. Strmcnik, P.P. Lopes, N.M. Markovic, Nat. Mater. 16 (2017) 57–69.
[11] C. Lv, C. Yan, G. Chen, et al., Angew. Chem. Int. Ed. 57 (2018) 6073–6076.
[12] Z.W. Seh, J. Kibsgaard, C.F. Dickens, et al., Science 355 (2017) eaad4998.
[13] M. Shao, Q. Chang, J.P. Dodelet, R. Chenitz, Chem. Rev. 116 (2016) 3594–3657.
[14] X.X. Wang, D.A. Cullen, Y.T. Pan, et al., Adv. Mater. 30 (2018) 1706758.
[15] X. Zhang, X. Cheng, Q. Zhang, J. Energy Chem. 25 (2016) 967–984.
[16] B.Y. Xia, Y. Yan, N. Li, et al., Nat. Energy 1 (2016) 15006.
[17] H.B. Yang, J. Miao, S.F. Hung, et al., Sci. Adv. 2 (2016) e1501122.
[18] S. Dou, A. Shen, L. Tao, S. Wang, Chem. Commun. (Camb.) 50 (2014) 10672–10675.
[19] L. Yang, X. Zeng, W. Wang, D. Cao, Adv. Funct. Mater. 28 (2018) 1704537.
[20] P. Yin, T. Yao, Y. Wu, et al., Angew. Chem. Int. Ed. 55 (2016) 10800–10805.
[21] J. Wu, S. Dou, A. Shen, et al., J. Mater. Chem. A Mater. Energy Sustain. 2 (2014) 20990–20995.
[22] V.M. Bau, X. Bo, L. Guo, J. Energy Chem. 26 (2017) 63–71.
[23] L. Hou, J. Guo, Z. Xiang, J. Energy Chem. 28 (2019) 73–78.
[24] W. Xia, A. Mahmood, Z. Liang, R. Zou, S. Guo, Angew. Chem. Int. Ed. 55 (2016) 2650–2676.
[25] B. Wang, X. Cui, J. Huang, R. Cao, Q. Zhang, Chin. Chem. Lett. 29 (2018) 1757–1767.
[26] Y. Gorlin, B. Lassalle-Kaiser, J.D. Benck, et al., J. Am. Chem. Soc. 135 (2013) 8525–8534.
[27] Z. Zhang, J. Liu, J. Gu, L. Su, L. Cheng, Energy Environ. Sci. 7 (2014) 2535–2558.
[28] T. Wang, J. Wu, Y. Liu, et al., Energy Storage Mater. 16 (2019) 24–30.
[29] Z. Hu, C. Chen, H. Meng, et al., Electrochem. commun. 13 (2011) 763–765.
[30] S. Li, B. Li, L. Ma, J. Yang, H. Xu, Chin. Chem. Lett. 28 (2017) 2159–2163.
[31] B. Yan, N.M. Concannon, J.D. Milshtein, F.R. Brushett, Y. Surendranath, Angew. Chem. Int. Ed. 56 (2017) 7496–7499.
[32] J. Xiao, Y. Xia, C. Hu, J. Xi, S. Wang, J. Mater. Chem. A Mater. Energy Sustain. 5 (2017) 11114–11123.
[33] J.L. Shi, C. Tang, J.Q. Huang, W. Zhu, Q. Zhang, J. Energy Chem. 27 (2018) 167–175.
[34] C. Tang, Q. Zhang, Adv. Mater. 29 (2017) 1604103.
[35] C. Tang, H.F. Wang, Q. Zhang, Accounts. Chem. Res. 51 (2018) 881–889.
[36] M. Zhou, H.L. Wang, S. Guo, Chem. Soc. Rev. 45 (2016) 1273–1307.
[37] Y. Liang, Y. Li, H. Wang, et al., Nat. Mater. 10 (2011) 780–786.
[38] C. Tang, M.M. Titirici, Q. Zhang, J. Energy Chem. 26 (2017) 1077–1093.
[39] J. Xie, B.Q. Li, H.J. Peng, et al., Angew. Chem. Int. Ed. 58 (2019) 4963–4967.
[40] M.L. Rigsby, D.J. Wasylenko, M.L. Pegis, J.M. Mayer, J. Am. Chem. Soc. 137 (2015) 4296–4299.
[41] W. Zhang, W. Lai, R. Cao, Chem. Rev. 117 (2017) 3717–3797.
[42] A.N. Oldacre, A.E. Friedman, T.R. Cook, J. Am. Chem. Soc. 139 (2017) 1424–1427.
[43] G. Luo, Y. Wang, Y. Li, Sci. Bull. (Beijing) 62 (2017) 1337–1343.
[44] S.C. Xu, B.C. Hu, W.Y. Zhou, C.G. Sun, Z.L. Liu, Chin. Chem. Lett. 23 (2012) 157–160.
[45] A.P. Cote, A.I. Benin, N.W. Ockwig, et al., Science 310 (2005) 1166–1170.
[46] P. Kuhn, M. Antonietti, A. Thomas, Angew. Chem. Int. Ed. 47 (2008) 3450–3453.
[47] E.L. Spitler, W.R. Dichtel, Nat. Chem. 2 (2010) 672–677.
[48] A. Bhunia, I. Boldog, A. Moeller, C. Janiak, J. Mater, Chem. A 1 (2013) 14990–14999.
[49] Y. Yuan, P. Cui, Y. Tian, et al., Chem. Sci. 7 (2016) 3751–3756.
[50] B.Q. Li, S.Y. Zhang, B. Wang, et al., Energy Environ. Sci. 11 (2018) 1723–1729.
[51] B.Q. Li, S.Y. Zhang, L. Kong, H.J. Peng, Q. Zhang, Adv. Mater. 30 (2018) 1707483.
[52] B.Q. Li, X.R. Chen, X. Chen, et al., Research 2019 (2019) 4608940.
[53] L. Kong, B.Q. Li, H.J. Peng, et al., Adv. Energy Mater. 8 (2018) 1800849.
[54] J.J. Xu, C.H. Xiao, S.J. Ding, Chin. Chem. Lett. 28 (2017) 748–754.
[55] C. Tang, H.F. Wang, X. Chen, et al., Adv. Mater. 28 (2016) 6845–6851.
[56] C. Tang, H.S. Wang, H.F. Wang, et al., Adv. Mater. 27 (2015) 4516–4522..